Nigerian Research Journal of Chemical Sciences (ISSN: 2682-6054)
Volume 14, Issue 2, 2026

Synthesis and Characterization of UiO-66 Metal-Organic Framework and Natural Coagulants for Turbidity Removal

*[1]Juliet Dingtsen Dodo, [1]Lawal Yakubu. Shaikarau, [1]Shangkum Yildun. Goji, [1]Saraya Yakubu Nyam, [2]Dauda Bala Azik , [3]Rabiat Abdullahi Lawal

[1]Department of Chemistry, Faculty of Natural Sciences,
University of Jos, Plateau State, Nigeria,

[2]Department of Science Laboratory Technology, Faculty of Natural Sciences,
University of Jos, Nigeria.

[3]National Open University of Nigeria (NOUN), Wase Study Centre, Plateau State, Nigeria.

Corresponding Author: dodojuliet1969@gmail.com

Accepted: *May 5, 2026.* **Published Online***: May 8, 2026*

ABSTRACT

Contamination of surface water by suspended particles poses significant challenges to water quality and public health. This study reports synthesis, and characterization, of Metal-Organic Framework (MOF) UiO-66, with *Moringa oleifera*, and *Azadirachta indica* as coagulants for potential application in turbidity removal from water. UiO-66 synthesized via solvothermal method using zirconium tetrachloride ($ZrCl_4$) and terephthalic acid (BDC) in N, N-dimethylformamide. Characterized by Fourier Transform Infrared (FTIR), X-Ray Diffraction (XRD), Scanning Electron Microscopy (SEM)/Energy Dispersive X-Ray (EDS) spectroscopy, Brunuer Emmett Teller (BET), and Thermogravimetric Analysis (TGA). FTIR confirmed O–H, N–H, C–H, C≡C, C=C, and C–O in all coagulants. XRD of UiO-66 revealed semi-crystalline structure, peaks at 2θ values of 9°, 19°, 27°, and 39°, corresponding to (001), (002), (110), and (100) planes, typical of MOFs. Phases includes Montmorillonite (63%), Muscovite (2.5%), Marialite (19%), and Silvialite (15%). SEM showed irregular, nanometer-sized particles, average of 64 nm uniform distribution. BET revealed mesoporous structures, pore diameters (1.7–3.5 nm). UiO-66 uniform pore size distribution peak at 2.6 nm, cumulative pore volume (0.045 cc/g). TGA demonstrated multi-stage thermal degradation (300–520°C), stability temperatures, 409°C (UiO-66), 427°C (*Moringa oleifera*), 388°C (*Azadirachta indica)*. EDS confirmed Si, Cl, Na, and S, small amounts (Fe, Al, and Mg). Structural integrity shows suitability of these materials for water treatment.

Keywords: Synthesis; Metal-Organic Framework; UiO-66; *Moringa oleifera*; *Azadirachta indica,* Characterization.

INTRODUCTION

Access to clean and safe water remains a critical global challenge, particularly in developing regions where surface water sources are often contaminated with suspended particles, organic matter, and pathogens [1]. Turbidity, a measure of water clarity, is a key indicator of water quality that affects aesthetic acceptability, disinfection efficiency, and public health [2].

Conventional water treatment methods, particularly coagulation-flocculation-sedimentation (CFS) processes, play a crucial role in removing turbidity and improving water quality [3]. However, traditional chemical coagulants such as aluminum sulfate (alum) have been associated with potential health risks, including neurotoxicity and Alzheimer's disease, and produce large volumes of non-biodegradable sludge [4, 5]. These limitations have driven research interest in alternative coagulants that are environmentally friendly, biodegradable, and cost-effective [6].

Natural coagulants derived from plant materials have gained significant attention due to their biodegradability, safety, and local availability [7, 8]. *Moringa oleifera* seeds have been extensively studied for their coagulation properties, attributed to water-soluble cationic proteins that act as natural polyelectrolytes, neutralizing negatively charged colloidal particles [9, 10]. The coagulant protein in Moringa seeds, identified as MO2.1 with molecular mass of approximately 6.5 kDa and isoelectric point above 10, has demonstrated turbidity removal efficiencies of 76–98% (Nhut et al., 2020) and bacterial removal exceeding 90% [11]. *Azadirachta indica* (neem) seeds have also shown potential as natural coagulants, containing bioactive compounds including triterpenes, flavonoids, and saponins that contribute to coagulation and antimicrobial activity [12, 13]. Studies have demonstrated that powdered neem seeds can achieve turbidity removal of up to 86% under optimized conditions [14]

Metal-Organic Frameworks (MOFs) represent a class of advanced porous materials that have emerged as promising candidates for water treatment applications [15]. Among various MOFs, UiO-66 (University of Oslo-66) has attracted particular attention due to its exceptional chemical and thermal stability, high surface area, tunable pore structure, and low cytotoxicity [16]. UiO-66 consists of zirconium (Zr^{4+}) clusters connected by terephthalic acid linkers, forming a

three-dimensional porous network with remarkable resistance to water, acids, and organic solvents [17]. These properties make UiO-66 suitable for adsorption and coagulation applications in water treatment.

In spite of the individual potential of these materials, comparative studies evaluating the structural properties and coagulation efficiency of MOFs alongside natural coagulants remain limited. This study addresses this research gap by: (i) synthesizing UiO-66 nanoparticles via solvothermal method; (ii) preparing *Moringa oleifera* and *Azadirachta indica* seed powders; (iii) comprehensively characterizing all materials using FTIR, XRD, SEM-EDX, BET, and TGA; and (iv) establishing structure-property.

MATERIALS AND METHODS

Materials

Zirconium tetrachloride ($ZrCl_4$, 99%), terephthalic acid (BDC, 98%), N, N-dimethylformamide (DMF, 99.8%), hydrochloric acid (HCl, 37%), methanol (CH_3OH, 99.5%), and ethanol were procured from Sigma-Aldrich. All reagents were of analytical grade and used without further 2.0 purification. Distilled water was obtained from the Pharmacy Laboratory, University of Jos.

Moringa oleifera Lam. Zogoole seeds (Voucher/Deposit no: JUHN2026:0091) were obtained from Shendam Local Government Area, and *Azadirachta indica* A. Juss. Dogon yaro (Voucher/Deposit Number: JUHN202600100) seeds were obtained from Langtang South Local Government Area, Plateau State, Nigeria. These seeds were authenticated at the Jos University Herberium Nigeria and the Voucher numbers obtained as stated above.

Synthesis of UiO-66 Nanoparticle

UiO-66 was synthesized using the solvothermal method following established procedures with modifications [18]. Specifically, 6.16 g of zirconium tetrachloride ($ZrCl_4$) and 4.4 g of terephthalic acid (BDC) were dissolved in 220 cm^3 of a mixture containing N, N-dimethylformamide (DMF), 2-propanol, and distilled water. The contents were stirred continuously for 30 minutes to ensure complete dissolution and homogeneous mixing. The resulting solution was transferred to a Teflon-lined autoclave and heated at 120°C for 5 hours under autogenous pressure. After completion of the reaction, the mixture was allowed to cool gradually to room temperature for 12–15 hours to promote crystal growth and stability. The white crystalline precipitate of UiO-66 nanoparticles was collected by centrifugation and washed repeatedly with methanol (MeOH) to remove unreacted

precursors and solvent molecules. The washed product was dried under vacuum at 80°C for 12 hours and stored in airtight containers for further characterization.

Preparation of Natural Coagulants

***Moringa oleifera* Seed Powder**

Matured dried *Moringa oleifera* seeds were manually separated from pods and foreign materials. The clean seeds were air-dried for several days to reduce moisture content, then crushed using a clean electric grinder to obtain coarse particles. The ground material was oven-dried at 40°C for 6 hours to remove residual moisture and sieved through a 0.42 mm mesh sieve to obtain uniform fine powder. The powder was stored in airtight opaque containers in a cool, dry place until use.

***Azadirachta indica* Seed Powder**

Riped *Azadirachta indica* seeds were collected, manually separated from husks, and thoroughly cleaned to remove impurities. The seeds were air-dried for one week, then crushed using an electric grinder. The crushed material was oven-dried at 40°C for 6 hours to ensure complete moisture removal and sieved through a 0.42 mm mesh sieve. The fine powder was stored in airtight containers for subsequent experiments.

Characterization

Fourier Transform Infrared Spectroscopy

FTIR spectra were recorded using a CARY 630 FTIR spectrometer in the range of 4000–400 cm^{-1} with a resolution of 4 cm^{-1}. Samples were analyzed directly to identify functional groups and chemical bonds present in UiO-66, *Moringa oleifera*, and *Azadirachta indica* .

X-ray Diffraction Analysis

XRD patterns were obtained using a Thermo Fisher Scientific ARL'XTRA X-ray diffractometer with Cu Kα radiation (λ = 1.5406 Å) operating at 40 kV and 40 mA. Data were collected over a 2θ range of 5–60° with a step size of 0.02°. Phase identification was performed by comparing obtained patterns with standard reference databases.

Scanning Electron Microscopy and Energy Dispersive X-ray Spectroscopy

Surface morphology and particle size distribution were examined using a JEOL GSM-IT810 Schottky Field Emission Scanning Electron Microscope operating at 10–20 kV accelerating

voltage. Samples were sputter-coated with gold to enhance conductivity. Elemental composition was determined using coupled EDS analysis.

Brunauer-Emmett-Teller Surface Area Analysis

Surface area, pore volume, and pore size distribution were determined by nitrogen adsorption-desorption isotherms at 77 K using a Micromeritics surface area analyzer. Samples were degassed at 150°C for 6 hours prior to analysis. Specific surface area was calculated using the BET method, while pore size distribution was determined using the Barrett-Joyner-Halenda (BJH) method.

Thermogravimetric Analysis

Thermal stability and decomposition behavior were investigated using a thermogravimetric analyzer under nitrogen atmosphere with a heating rate of 10°C/min from room temperature to 800°C. Sample masses of approximately 10 mg were used for each analysis.

RESULTS AND DISCUSSION

Figure 1 presents the FTIR spectrum of UiO-66 nanoparticle showing the various bands of absorption.

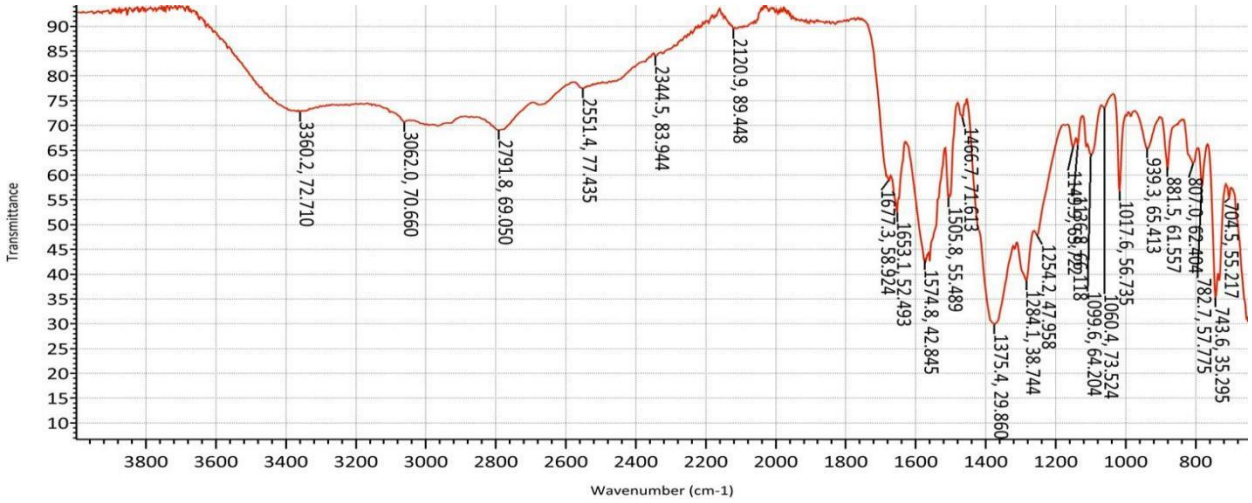

Figure 1: FTIR Spectrum of UiO-66 Nanoparticles

Table 1 shows the functional groups present in UiO-66 nanoparticle with their corresponding wave numbers. The highest wave number was 3335.3 cm^{-1} and lowest was 743.5 cm^{-1}.

Table 1: Functional Groups present in UiO-66

Wavenumber (cm^{-1})	Possible Functional Group / Vibration
3335.3	O–H or N–H stretch (alcohols, amines) — broad if O–H
2851.1 - 2957.1	C–H stretch (alkanes)
2137.5	C≡C or C≡N stretch (alkynes or nitriles)
1735.3	C=O stretch (strong, indicative of ketones, esters, aldehydes)
1603.3	C=C stretch (aromatic ring)
1456.7 - 1486.3	CH_2/CH_3 bending (alkanes), C=C stretch (aromatic)
1235.1	C–O stretching (esters or ethers)
1167.6 - 1386.2	C–O stretch (ethers, esters, alcohols) or C–N stretch (amines)
1004.4	Aromatic C–H in-plane bending
983.3	=C–H bending (alkenes) or C–H wag (alkyl halides)
743.5 - 881.5	C-H out-of-plane bending (aromatic rings or alkenes)

The FTIR spectrum of synthesized UiO-66 nanoparticles revealed characteristic absorption bands confirming successful formation of the metal-organic framework. The broad band at 3335.3 cm^{-1} corresponds to O–H stretching vibrations from adsorbed water molecules and possible N–H stretches from residual solvent, indicating the hydrophilic nature of the MOF surface [19]. The bands in the region 2851.1–2957.1 cm^{-1} are attributed to asymmetric and symmetric C–H stretching vibrations of aliphatic groups from the organic linker.

The strong band at 1735.3 cm^{-1} represents C=O stretching vibrations of the carboxylic acid groups in terephthalic acid, confirming the presence of the organic linker. The bands at 1603.3 cm^{-1} and 1456.7–1486.3 cm^{-1} correspond to C=C stretching vibrations of the aromatic ring, confirming the structural integrity of the benzene dicarboxylate linker. The bands in the region 1167.6–1386.2 cm^{-1} are characteristic of C–O stretching vibrations and C–N stretches, indicating successful coordination between the zirconium clusters and carboxylate groups [20]. The presence of bands at 743.5–881.5 cm^{-1} corresponding to C–H out-of-plane bending of aromatic rings further confirms the incorporation of the organic linker. These spectral features are consistent with previously reported UiO-66 spectra [21, 22], confirming successful synthesis of the MOF structure.

Figure 2 is the FTIR spectrum of *Moringa oleifera* showing the peaks of absorptions at different wave numbers.

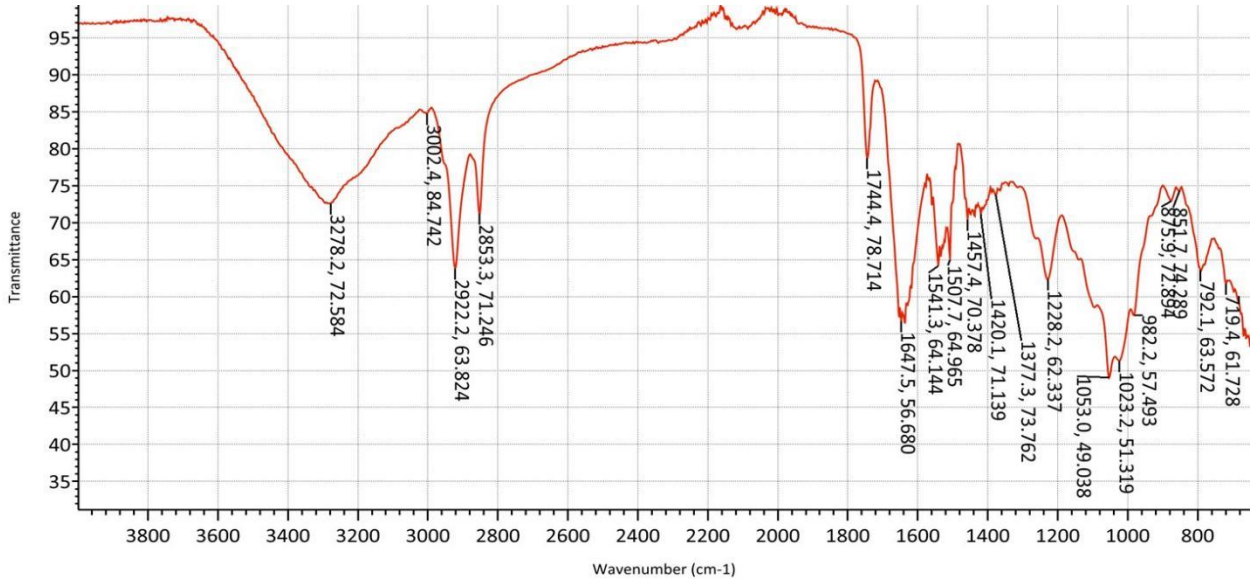

Figure 2: FTIR Spectrum of *Moringa oleifera*

Table 2 presents the functional groups in *Moringa oleifera.* The highest wave number was 3278.2 cm^{-1} for broad absorption of alcohol and sharp absorption for the amines, while the lowest absorption band was at 719.4 cm^{-1} corresponding to the aromatics or alkenes.

Table 2: Functional Groups Present in *Moringa oleifera.*

Wavenumber (cm^{-1})	Functional Group Present
3278.2	O–H or N–H stretch (broad if alcohol; sharp if amine)
3002.4	=C–H stretch (alkenes or aromatics)
2853.3 – 2922.2	C–H stretch (alkanes: symmetric and asymmetric)
1744.4	C=O stretch (very strong, typical of esters, ketones, aldehydes)
1541.3 – 1647.5	C=C stretch (aromatic), N–H bending (amines), possible nitro compounds
1420.1 – 1507.7	C–C stretching (aromatics), CH_2 bending (alkanes), possible N–H bending
1377.3	CH_3 symmetric bending (alkanes), also possible nitro group
1023.2 – 1228.2	C–O stretch (ethers, esters, alcohols), also C–N (amines)
851.7 – 982.2	C–H wagging, twisting (alkyl halides, alkenes)
792.1	C–H out-of-plane bending (aromatics or substituted alkenes)
719.4	C–H out-of-plane bending (aromatics or alkenes)

The FTIR spectrum of *Moringa oleifera* seed powder revealed complex organic composition characteristic of plant materials. The broad band at 3278.2 cm^{-1} indicates O–H and N–H stretching vibrations from alcohols, phenols, and amines, corresponding to proteins and carbohydrates present in the seeds [23; 24]. The bands at 2853.3–2922.2 cm^{-1} represent C–H stretching of aliphatic compounds including lipids and proteins.

The strong band at 1744.4 cm^{-1} is characteristic of C=O stretching of ester carbonyl groups, indicating the presence of oils and fatty acids in the seeds. The bands at 1541.3–1647.5 cm^{-1} correspond to amide I and II vibrations from protein structures, confirming the presence of the

cationic coagulant protein MO2.1 responsible for coagulation activity [10]. The bands in the region 1023.2–1228.2 cm^{-1} represent C–O stretching of carbohydrates and C–N stretching of amines, indicating the presence of polysaccharides and proteins. The presence of these functional groups confirms the complex biochemical composition of Moringa seeds that contributes to their coagulation and antimicrobial properties [25].

Figure 3 presents the FTIR spectrum of *Azadirachta indica* showing the various absorption peaks with their wave numbers in the sample, whereas Table 3 shows the functional groups.

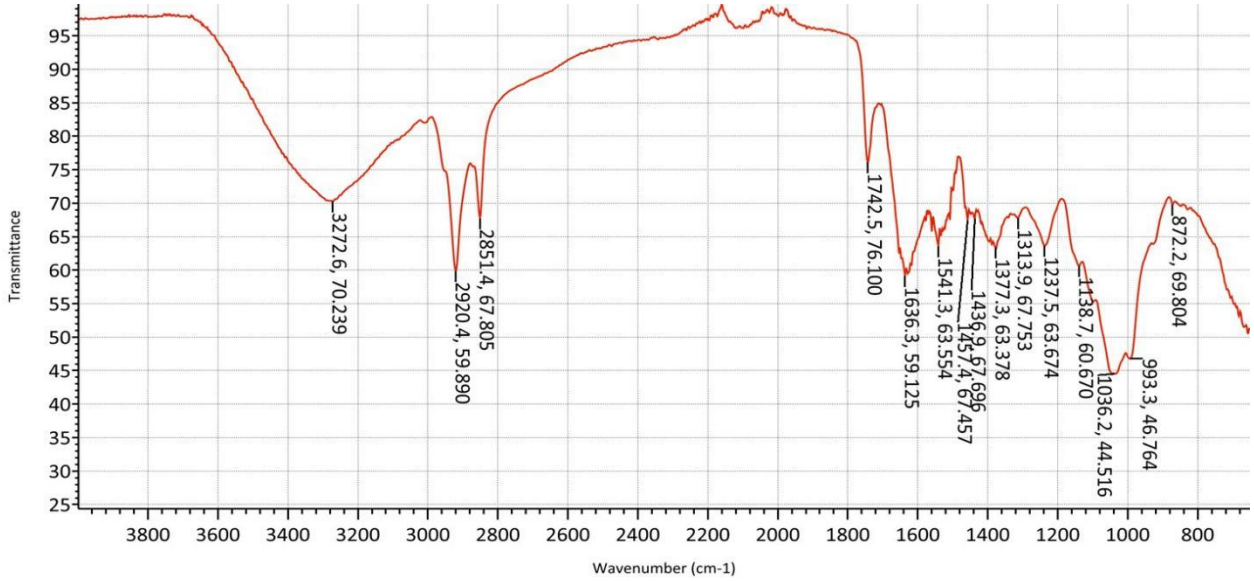

Figure 3: FTIR Spectrum of *Azadirachta indica*

Table 3: Functional Groups Present in *Azadirachta indica*

Wavenumber (cm^{-1})	Possible Functional Group / Bond Vibration
3272.6	N–H or O–H stretch (amines or alcohols)
2851.4 – 2920.4	C–H stretch (alkanes, symmetric & asymmetric)
1742.5	C=O stretch (strong — esters, aldehydes, ketones)
1636.3	C=C stretch (alkenes/aromatics), or amide N–H bending
1436.9 – 1541.3	C–C stretch (aromatics), N–H bending (amines), nitro

1457.4	CH_2 bending (alkanes), aromatic ring deformation
1313.9 – 1377.3	CH_3 bending (alkanes), possible S=O or nitro group
1036.2 – 1237.5	C–O stretch (alcohols, ethers), C–N (amines)
993.3	=C–H bending (alkenes), possibly C–O stretching
872.2	C–H out-of-plane bending (aromatics or alkenes)

The FTIR spectrum of *Azadirachta indica* seed powder revealed characteristic functional groups consistent with its complex phytochemical composition. The broad band at 3272.6 cm^{-1} indicates O–H and N–H stretching vibrations from various bioactive compounds including triterpenes, flavonoids, and alkaloids [26]. The bands at 2851.4–2920.4 cm^{-1} correspond to C–H stretching of aliphatic compounds.

The band at 1742.5 cm^{-1} represents C=O stretching of ester and carbonyl groups, indicating the presence of limonoids and other terpenoid compounds characteristic of neem [27]. The bands at 1636.3 cm^{-1} and 1436.9–1541.3 cm^{-1} correspond to C=C stretching of aromatic rings and N–H bending of amines, confirming the presence of flavonoids and nitrogen-containing compounds. The bands in the region 1036.2–1237.5 cm^{-1} represent C–O stretching of alcohols and ethers, and C–N stretching of amines, consistent with the presence of carbohydrates and alkaloids [28]. These functional groups contribute to the coagulation and antimicrobial properties of neem seeds, as reported in previous studies by [29; 30].

Figure 4 is the XRD pattern of UiO-66 nanoparticle at the various intensities and the 2 theta values.

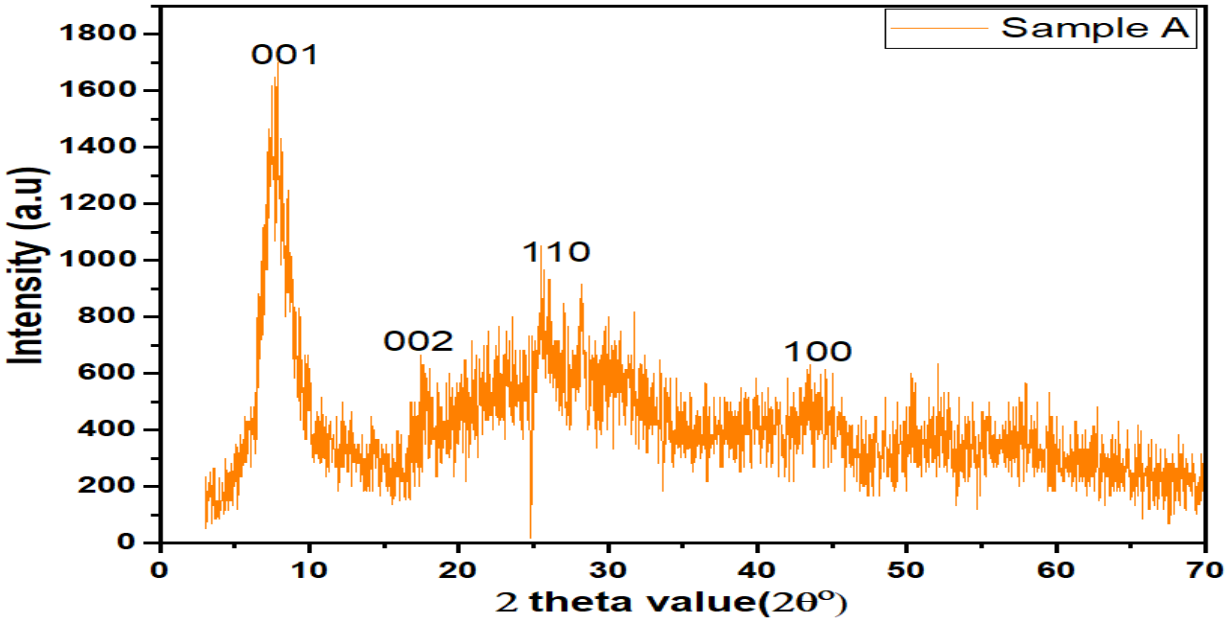

Figure 4: XRD pattern of UiO-66 Nanoparticles

Table 4 presents the observations from the XRD pattern of UiO-66 nanoparticles at the various 2θ values and the corresponding intensities. The interpretation of these observations is also highlighted as remarks.

Table 4: Observations from XRD Pattern of UiO-66 Nanoparticles

2θ (°)	Intensity (a.u.)	Miller Indices (hkl)	Remarks
9.00°	~1700	(001)	Strong basal reflection indicating layered structure
19.00°	~600	(002)	Second-order reflection, confirming periodicity
27.00°	~1000	(110)	Suggests in-plane ordering, possible rhombohedral phase
39.00°	~600	(100)	Indicates further crystallographic alignment

Figure 4 presents the percentage amount of detected compounds in UiO-66 Nanoparticles. Montmorillonite had the highest of 63% while silvialite had the lowest of 15%.

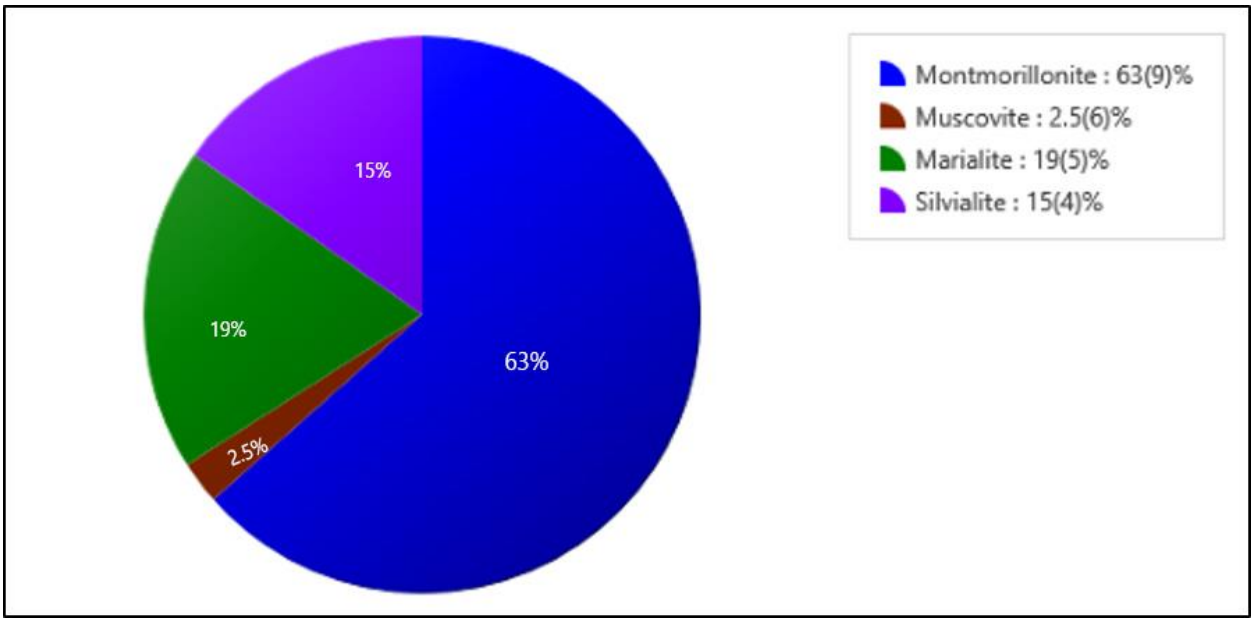

Figure 5: The percentage amount of detected compounds in UiO-66 Nanoparticles

The X-ray diffraction pattern of UiO-66 revealed distinct peaks characteristic of the MOF structure. The strong reflection at 2θ = 9.00° with intensity ~1700 a.u. corresponds to the (001) plane, indicating well-defined interlayer spacing typical of layered MOF structures [31]. This strong basal reflection suggests ordered stacking of the framework layers. The peak at 2θ = 19.00° (~600 a.u.) corresponds to the (002) plane, confirming periodic repetition in the c-axis direction. The reflection at 2θ = 27.00° with intensity ~1000 a.u. represents the (110) plane, indicating in-plane ordering within the framework structure. The peak at 2θ = 39.00° (~600 a.u.) corresponds to the (100) plane, suggesting additional crystallographic alignment. The broadened nature of peaks beyond 20.00° indicates nanocrystallinity and the presence of some amorphous domains, which is characteristic of solvothermally synthesized UiO-66 nanoparticle [32].

Phase identification revealed multiple crystalline components in the synthesized material. Montmorillonite was identified as the dominant phase (63.0%), appearing at 2θ = 9.00° corresponding to DB card no. 00-002-0037. Muscovite (2.50%) was identified at 2θ = 19.00° (DB card no. 00-001-1098). Marialite (19.0%) appeared at 2θ = 27.00° (DB card no. 00-002-0412), and Silvialite (15.0%) at 2θ = 39.00° (DB card no. 00-002-0405). The presence of these phases

suggests the formation of a complex composite structure with potential synergistic properties for water treatment applications.

Figure 6 is the SEM spectrum and the particle size distribution of UiO-66 nanoparticle. The highest particle size was 110 nm

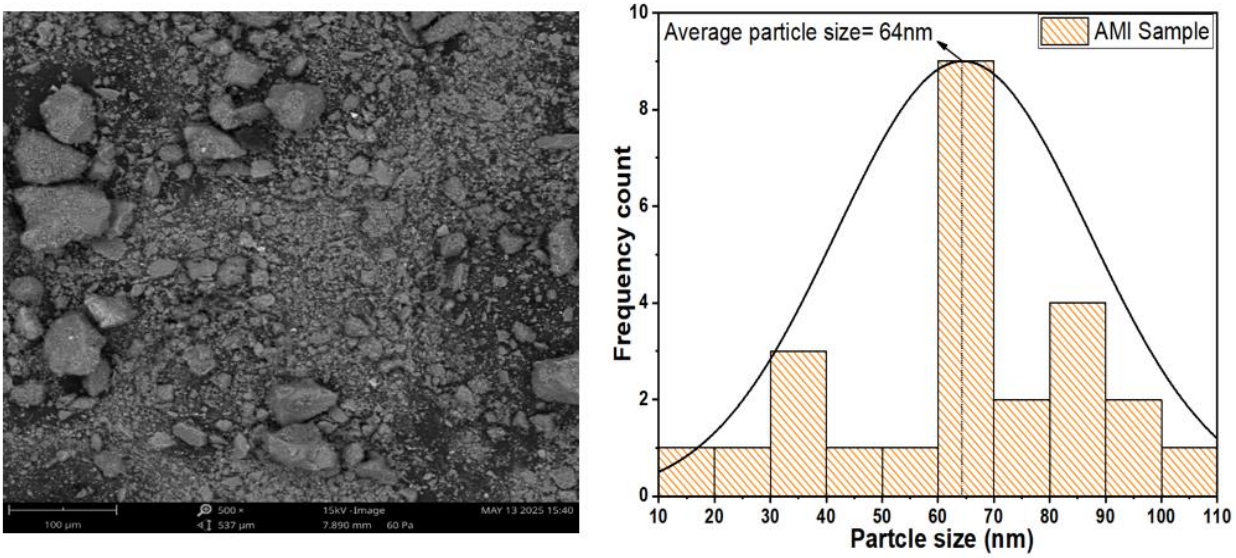

Figure 6: SEM Spectrum and Particle size distribution for UiO-66 Nanoparticles

Figure 7 is the EDS pattern for UiO-66 Nanoparticle, its Elemental composition, their atomic concentrations and weight concentration. Ca, Ti, V, Mn and P were absent in this nanoparticle.

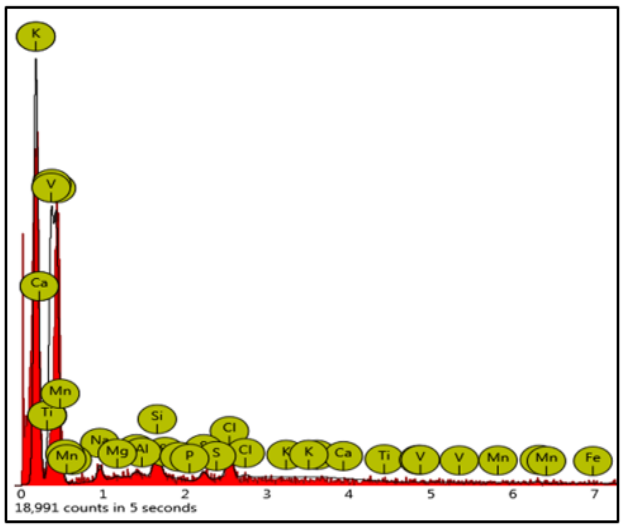

Element Number	Element Symbol	Element Name	Atomic Conc.	Weight Conc.
17	Cl	Chlorine	29.04	33.47
14	Si	Silicon	32.43	29.60
11	Na	Sodium	18.37	13.73
16	S	Sulfur	9.37	9.76
26	Fe	Iron	4.42	8.02
13	Al	Aluminium	4.37	3.83
12	Mg	Magnesium	2.01	1.59
20	Ca	Calcium	0.00	0.00
19	K	Potassium	0.00	0.00
22	Ti	Titanium	0.00	0.00
23	V	Vanadium	0.00	0.00
25	Mn	Manganese	0.00	0.00
15	P	Phosphorus	0.00	0.00

Figure 7: EDS pattern for UiO-66 Nanoparticle and Its Elemental composition

SEM analysis revealed that the synthesized UiO-66 consists of predominantly irregular, nanometer-sized particles with an average size of 64 nm. The particle size distribution is relatively uniform, ranging from approximately 20 nm to 100 nm, with a slight tendency toward smaller particles. The histogram shows a normal distribution curve centered around 60–70 nm, indicating controlled particle growth during synthesis.

The particles exhibit irregular morphology with angular features and some sub-rounded edges. Surfaces show a rough texture, indicating minimal smoothing or rounding, which is typical for solvothermally synthesized MOF materials. Moderate aggregation is observed, with some particles appearing as clusters or agglomerates, while others are well-dispersed. The observed morphology and particle size distribution are consistent with previously reported UiO-66 syntheses [21, 33].

The nanometer-scale particle size (<100 nm) and relatively narrow size distribution are advantageous for coagulation applications, as smaller particles provide higher surface area and enhanced interaction with colloidal contaminants. The irregular morphology and rough surface texture increase the effective surface area available for adsorption and particle bridging during coagulation [34].

EDS analysis revealed the elemental composition of the synthesized UiO-66 nanoparticle. The spectrum shows prominent peaks corresponding to silicon, chlorine, sodium, sulphur, with minor peaks for iron, aluminum, and magnesium. Quantitative analysis indicates that silicon and chlorine are the most abundant elements, together comprising over 60% of the atomic composition. Sodium and sulfur are present in significant amounts, while iron, aluminum, and magnesium are present in minute quantities. Elements including calcium, potassium, titanium, vanadium, manganese, and phosphorus were not detected in the sample, indicating concentrations below the detection limit of the EDS instrument used. The elemental composition suggests the sample may contain silicate phases with significant halide and sulphate content, consistent with the XRD identification of montmorillonite and other aluminosilicate phases. The presence of these elements indicates the formation of a complex composite material incorporating the MOF structure with mineral phases.

Table 5 shows the comparison between the parameters for the three absorbent studied, UiO-66 nanoparticle, *Moringa oleifera* and *Azadirachta indica* in terms of pore diameter,, pore type, cummulative pore volume, peak pore diameter and the dV/dD Peak Characteristics.

Table 5: Comparison between BET Results of UiO-66 nanoparticle, *Moringa oleifera* and *Azadirachta indica* samples

Parameter	UiO-66 Nanoparticle	*Moringa oleifera*	*Azadirachta indica*
Pore Diameter Range	1.7 – 2.8 nm	~2.0 – 3.2 nm	~2.1 – 3.5 nm
Pore Type	Mesoporous (close to microporous)	Mesoporous	Mesoporous
Cumulative Pore Volume	0.045 cc/g	Moderate increase (not numerically specified)	Slightly higher than Sample A (approx. 0.050 cc/g, estimated)
Peak Pore Diameter	2.6 nm	2.7 nm	2.8 nm
dV/dD Peak Characteristics	Sharp peak at 2.6 nm indicating dominant mesopore structure	Multiple peaks near 2.7 nm	Broader distribution peaking at 2.8 nm

Figure 8 shows the pore size of UiO-66 Nanoparticle

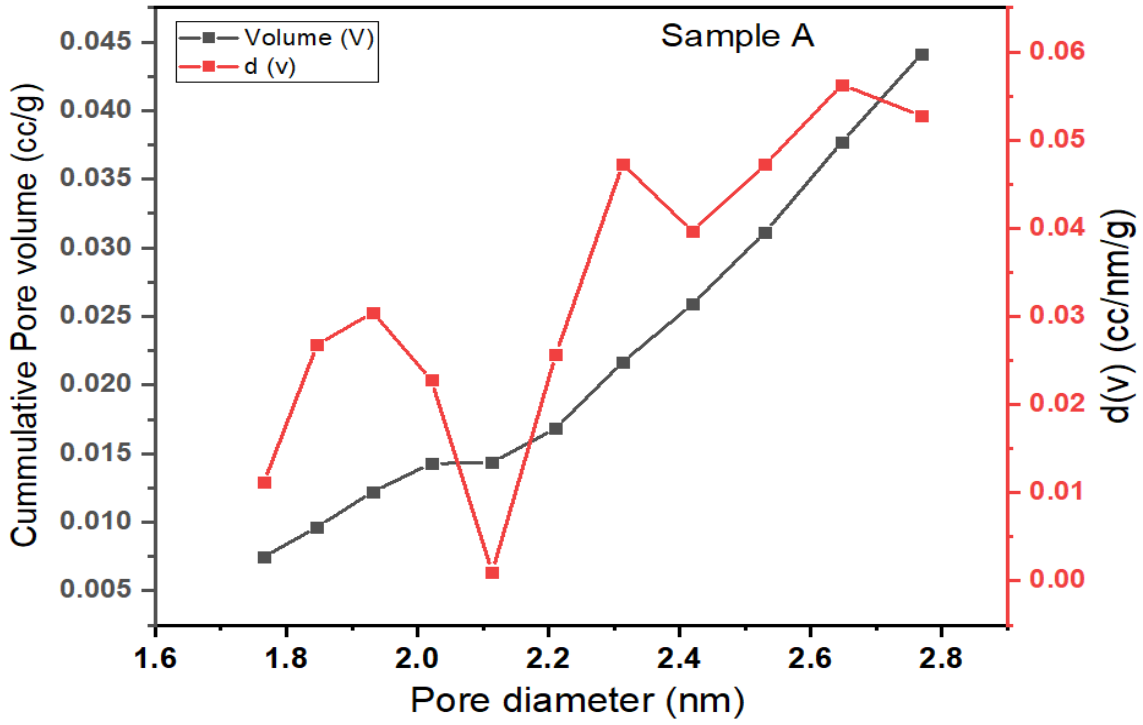

Figure 8: Pore size of UiO-66 Nanoparticle

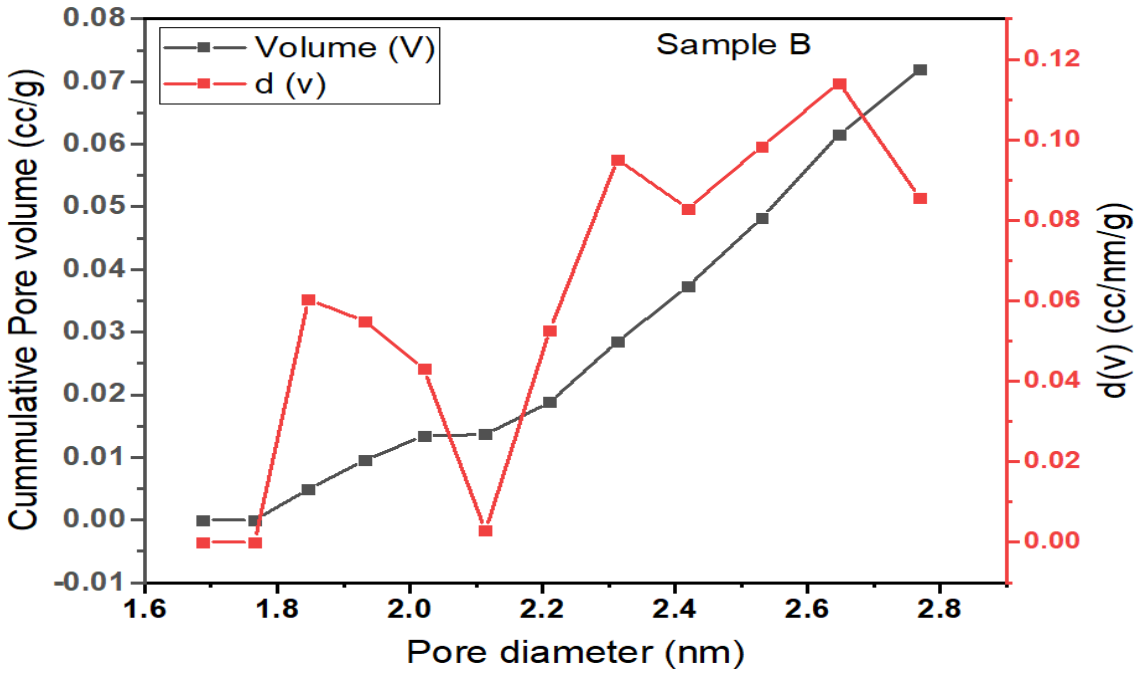

Figure 9: Pore Size of *Moringa oleifera*

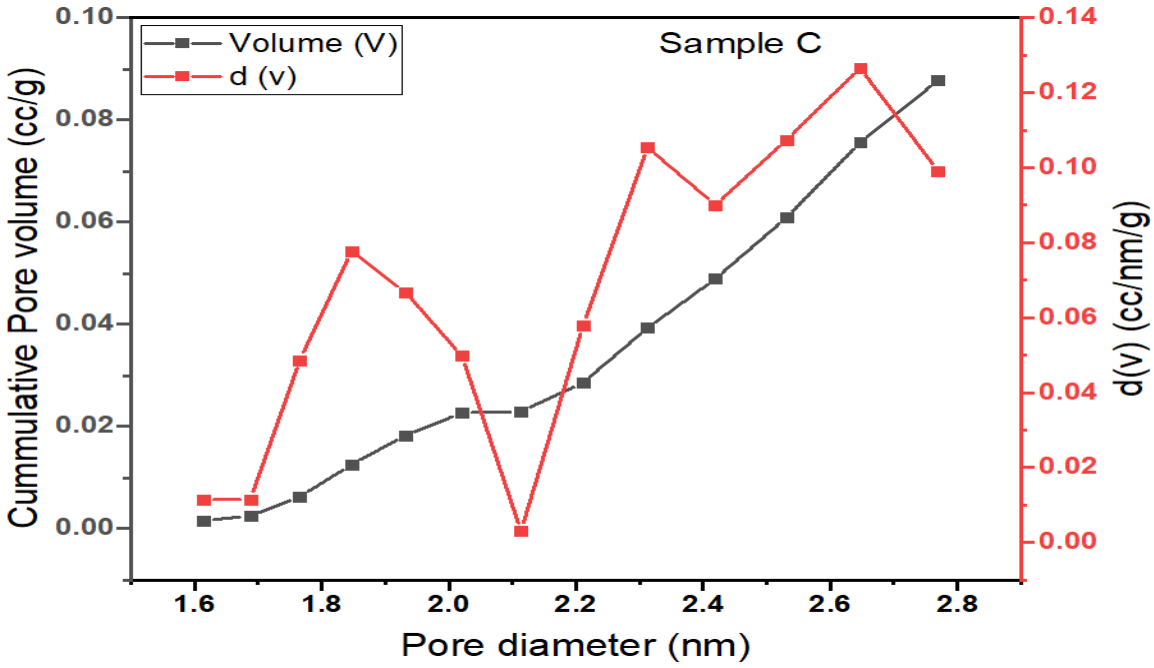

Figure 10: Pore size of *Azadirachta indica*

BET surface area analysis revealed distinct textural properties for the three coagulants. UiO-66 nanoparticle exhibited a narrow pore diameter range between 1.7 and 2.8 nm, classified within the mesoporous domain and bordering the microporous threshold. The dominant peak pore diameter at 2.6 nm indicates a uniform mesoporous structure, supported by a cumulative pore volume of 0.045 cc/g and sharp dV/dD peaks. These characteristics suggest that UiO-66 nanoparticle possesses a well-defined mesoporous architecture ideal for adsorption and coagulation applications, facilitating efficient mass transport and contaminant capture [35].

Moringa oleifera showed a slightly broader pore diameter distribution estimated between 2.0 and 3.2 nm, with multiple mesoporous peaks and a dominant pore size around 2.7 nm. The mesoporous character and moderate surface area are inferred from the dV/dD profile, indicating a less uniform pore network compared to UiO-66 nanoparticle. This broader pore distribution may enhance accessibility of active sites while maintaining good adsorption capacity.

Azadirachta indica displayed an even broader pore distribution ranging from approximately 2.1 to 3.5 nm, with a dominant pore diameter of 2.8 nm. The cumulative pore volume was slightly higher than that of UiO-66 nanoparticle (approximately 0.050 cc/g), with dV/dD peaks more broadly distributed, suggesting a more heterogeneous pore structure. This

broader pore distribution may enhance surface reactivity, making it suitable for adsorption-driven applications where diverse pore sizes facilitate capture of varying contaminant sizes.

The BET analysis reveals that all three samples exhibit mesoporous structures, but with different degrees of uniformity and volume. UiO-66 nanoparticle showed the most well-defined and narrow pore size distribution, making it particularly suitable for applications requiring uniform pore architecture such as size-selective adsorption and catalysis. *Moringa oleifera* and *Azadirachta indica* , showed broader pore distributions, which may offer advantages in applications where heterogeneous pore structures enhance overall surface reactivity.

Table 6 presents the comparison between the TGA values for UiO-66 nanoparticle, *Moringa oleifera* and *Azadirachta indica* showing the weight loss during decomposition .

Table 6: Comparison between TGA Results of UiO-66 nanoparticle, *Moringa oleifera* and *Azadirachta indica* samples.

Parameter	UiO-66 nanoparticle	*Moringa oleifera*	*Azadirachta indica*
Initial Decomposition Temp	305°C	~310°C	~298°C
First Major Weight Loss	Begins at 305°C, 95% wt. remaining	Begins at 310°C, 94% wt. remaining	Begins at 298°C, 92% wt. remaining
Second Major Weight Loss	Starts at 408°C, 57% wt. remaining	Starts at ~415°C, 55% wt. remaining	Starts at ~405°C, 52% wt. remaining
Final Residue Temperature	514°C, 11% wt. remaining	520°C, ~9% wt. remaining	515°C, ~7% wt. remaining
Thermal Stability	Moderate thermal stability, multi-stage	Slightly higher thermal stability	Slightly lower thermal stability

Figure 11 is graphical representation of the weight loss of UiO-66 nanoparticle with the percentage loss.

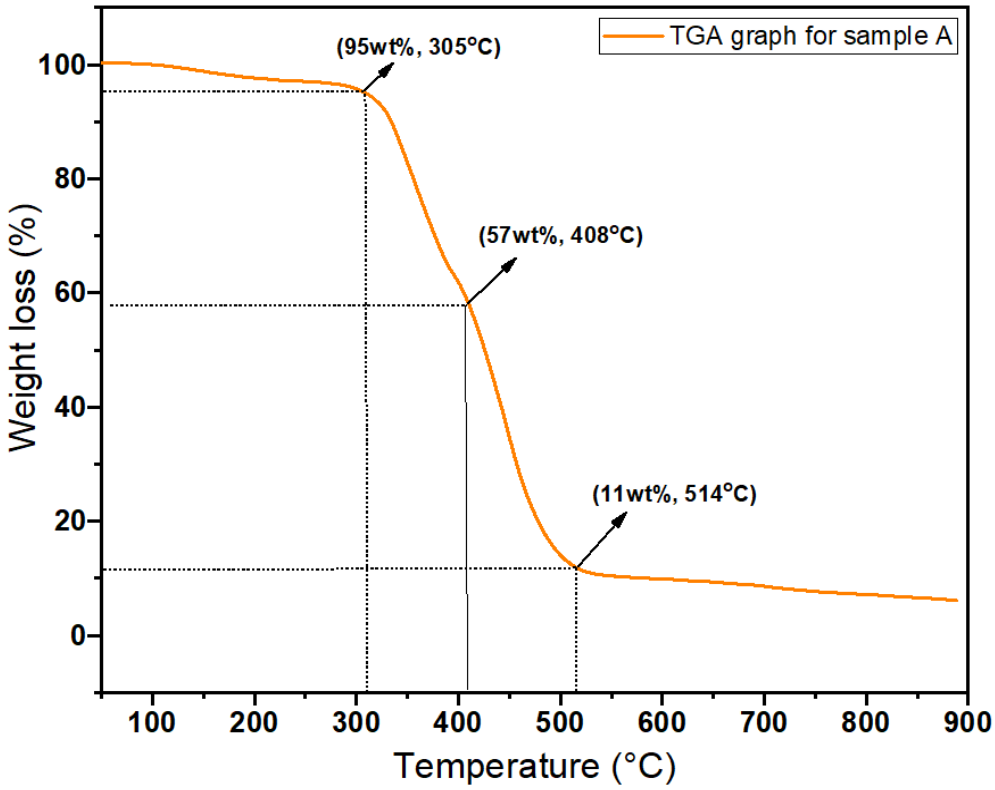

Figure 11: Weight Loss Pattern in UiO-66 Nanoparticle

Figure 12 shows the graphical representation of weight loss of *Moringa oleifera* with the percentages

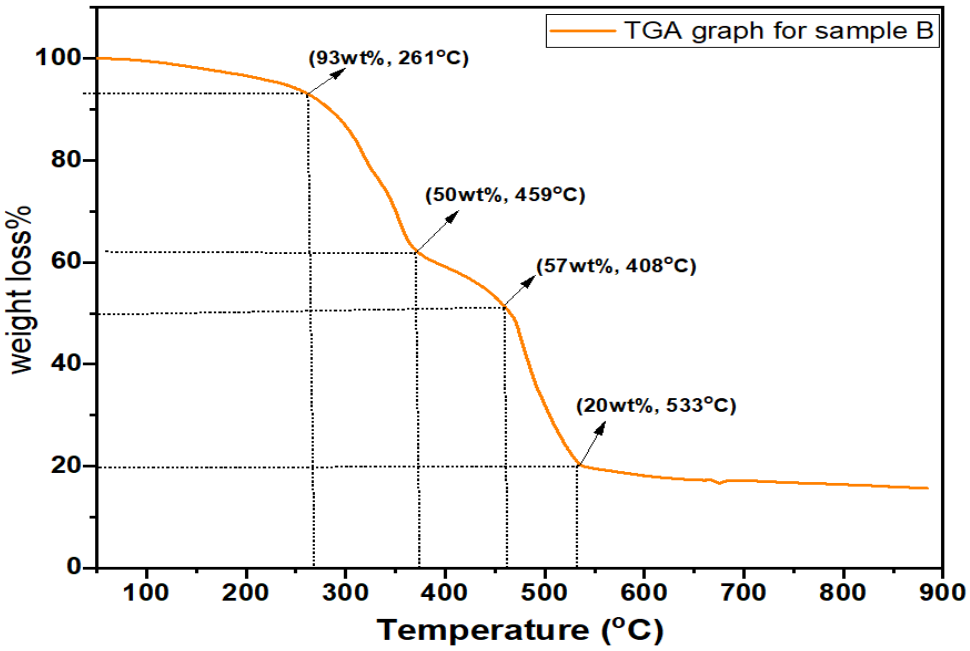

Figure 12: Weight Loss Pattern in *Moringa oleifera*

Figure 13 presents the graphical decomposition and weight loss of *Azadirachta indica* and the percentage loss.

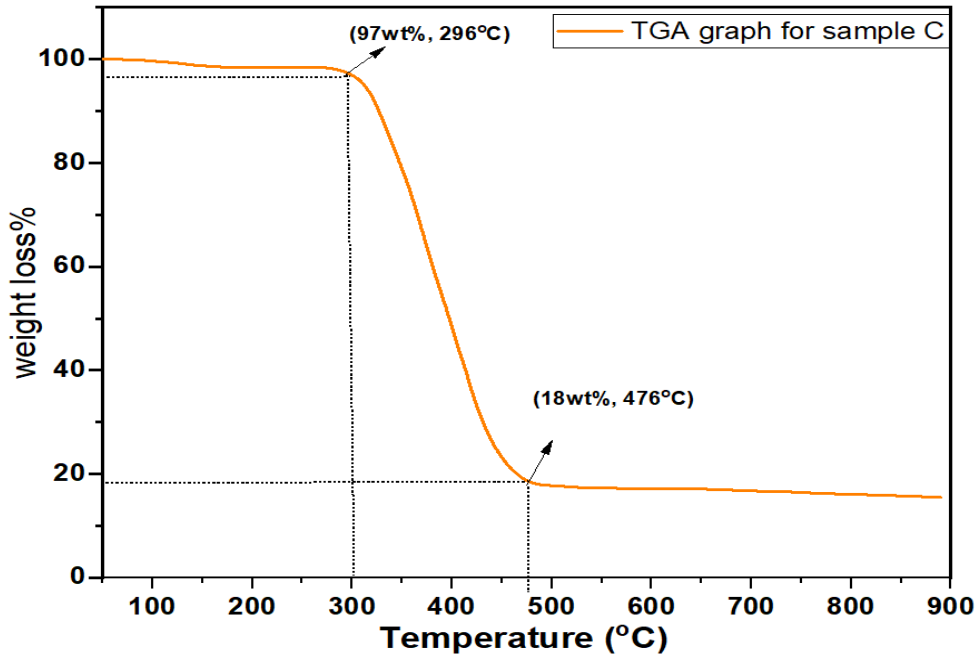

Figure 13: Weight Loss Pattern in *Azadirachta indica*

Table 7 presents the Maximum stability temperatures of the samples of adsorbents studied.

Table 7: Maximum Stability of A (UiO-66), B (*Moringa oleifera)*, C (*Azadirachta indica)*

Samples	Maximum Stability (°C)
UiO-66 nanoparticle	409
Moringa oleifera	427
Azadirachta indica	388

Figures 14 - 16 show the derivative weight loss of the UiO-66, *Moringa oleifera* and *Azadirachta indica* .

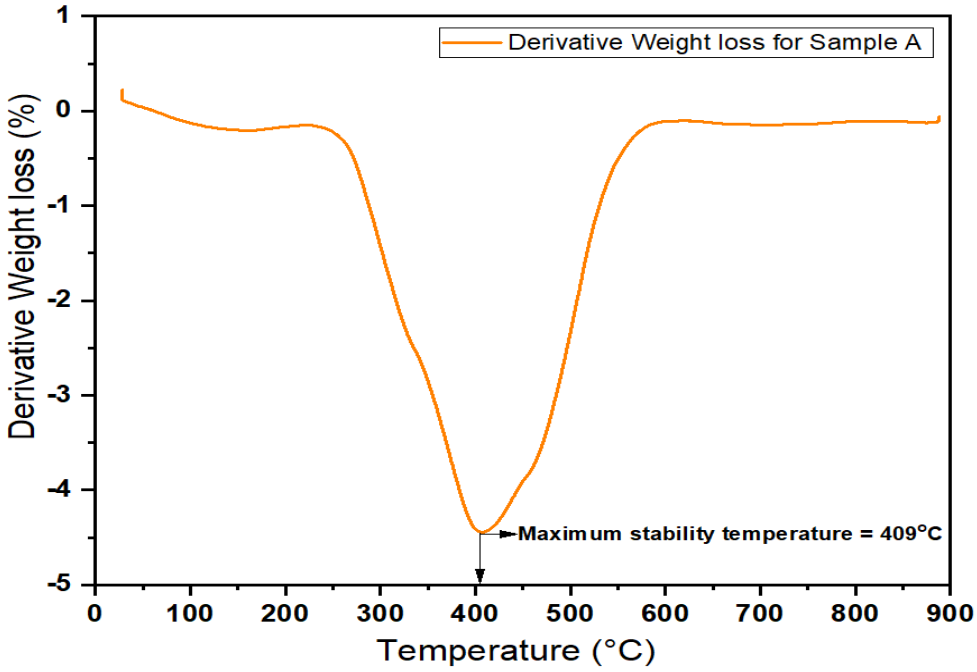

Figure 14: Derivatives Weight Loss of UiO-66 Nanoparticle

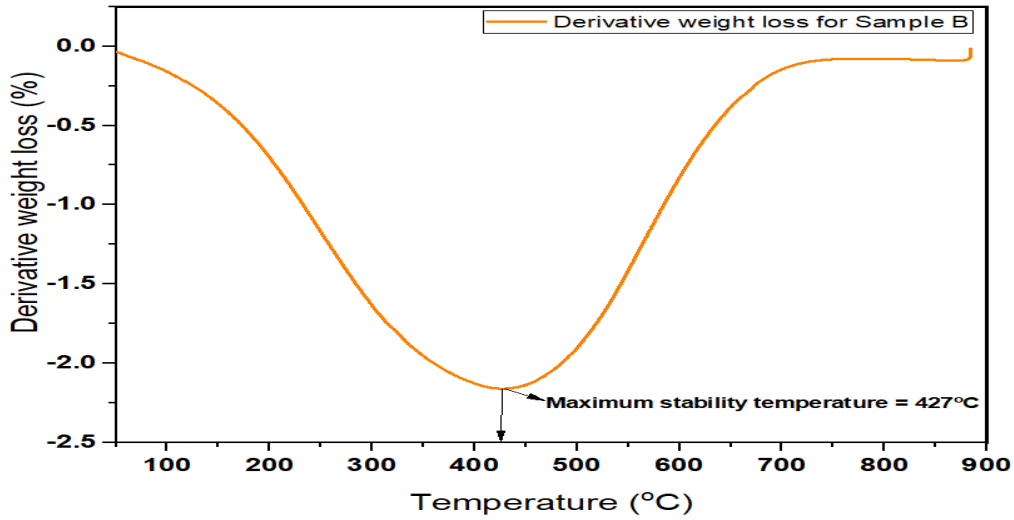

Figure 15: Derivatives Weight Loss of *Moringa oleifera*

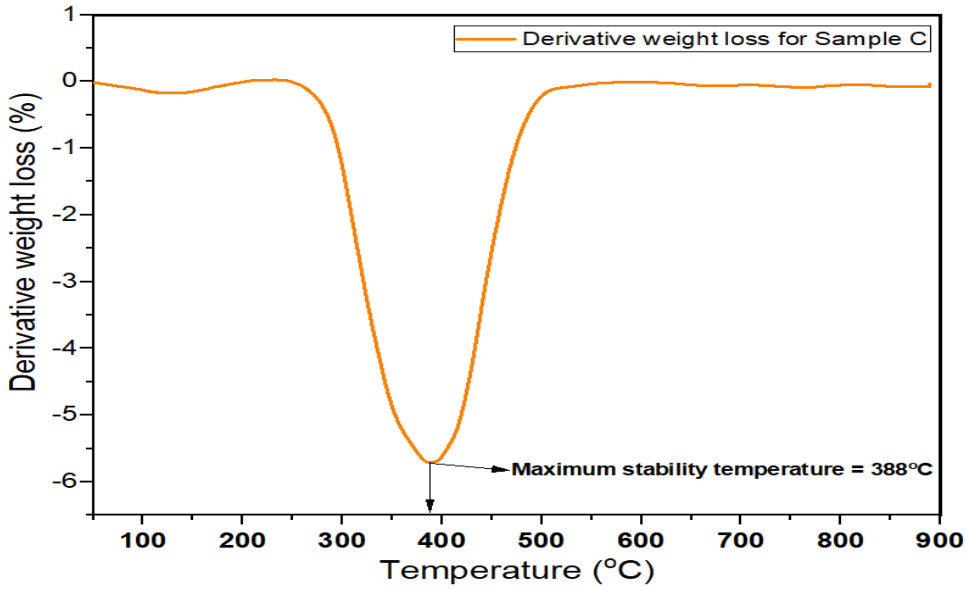

Figure 16: Derivatives Weight Loss of *Azadirachta indica* .

Thermogravimetric analysis provided insights into the thermal stability and decomposition behavior of the three coagulants. UiO-66 nanoparticle began to lose weight at 305°C, marking the onset of major decomposition, with 95% of initial weight retained at this stage. The second major weight loss occurred at 408°C, leaving 57% of the sample mass. By 514°C, only 11% of the original weight remained, indicating significant two-step degradation and moderate thermal

stability characteristic of MOF structures [36]. The maximum stability temperature for UiO-66 nanoparticle was 409°C.

Moringa oleifera initiated thermal degradation slightly later, around 310°C, with 94% of the sample remaining at this temperature. A second significant mass loss occurred around 415°C, and by 520°C, only 9% of the sample remained. This profile suggests that Moringa is slightly more thermally stable than UiO-66 nanoparticle, possibly due to its complex organic matrix containing thermally resistant components including proteins and lignocellulosic materials. The maximum stability temperature for *Moringa oleifera* was 427°C, the highest among the three samples.

Azadirachta indica began to decompose at a lower temperature of 298°C, with 92% of the weight retained. Further degradation occurred at approximately 405°C, with final residual mass at 515°C of about 7%. These figures point to higher volatility and lower thermal stability compared to UiO-66 nanoparticle and *Moringa oleifera*, likely due to a higher concentration of volatile organic compounds and less thermally stable phytochemicals [37]. The maximum stability temperature for *Azadirachta indica* was 388°C. Derivative weight loss analysis confirmed the multi-stage degradation patterns for all samples, with distinct peaks corresponding to decomposition of different components. The thermal degradation of all three samples occurs primarily between 300°C and 520°C. Moringa shows slightly higher thermal stability than UiO-66 particle and *Azadirachta indica* , while *Azadirachta indica* has the highest mass loss, indicating a larger proportion of volatile or organic content. These thermal stability characteristics are important considerations for material processing, regeneration, and application in water treatment under varying temperature conditions.

CONCLUSIONS

This study successfully synthesized and comprehensively characterized UiO-66 nanoparticle alongside *Moringa oleifera* and *Azadirachta indica* seed powders as potential coagulants for water treatment applications. UiO-66 nanoparticles were successfully synthesized via the solvothermal method, yielding crystalline material with an average particle size of 64 nm and a relatively uniform size distribution. Structural confirmation through FTIR analysis revealed characteristic functional groups for all materials: UiO-66 nanoparticle exhibited typical MOF vibrations including O–H, C=O, C=C, and C–O stretches; *Moringa oleifera* displayed protein-related amide bands (1541–1647 cm^{-1}) confirming the presence of coagulant proteins; while *Azadirachta indica*

showed characteristic bands of triterpenes and flavonoids at 1636 cm^{-1} and 1742 cm^{-1}. XRD analysis further revealed UiO-66 nanoparticle semi-crystalline layered structure with distinct reflections at $2\theta = 9°$, 19°, 27°, and 39°, corresponding to the (001), (002), (110), and (100) planes. Phase identification indicated a composite material containing montmorillonite (63%), marialite (19%), silvialite (15%), and muscovite (2.5%).

BET confirmed mesoporous structures for all materials, with UiO-66 nanoparticle exhibiting the most uniform pore size distribution (peak at 2.6 nm) and a pore volume of 0.045 cc/g. *Moringa oleifera* and *Azadirachta indica* showed broader pore distributions ranging from 2.0 to 3.5 nm with slightly higher pore volumes, offering complementary textural properties for diverse adsorption applications. Thermogravimetric analysis revealed multi-stage thermal degradation between 300–520°C, with maximum stability temperatures of 409°C for UiO-66, 427°C for *Moringa oleifera*, and 388°C for *Azadirachta indica* , confirming adequate thermal stability for water treatment applications under ambient conditions. EDS analysis confirmed the complex elemental composition of the synthesized materials, dominated by silicon, chlorine, sodium, and sulfur, with minor amounts of iron, aluminum, and magnesium, consistent with the composite nature of the materials.

The characterization establishes the structural integrity and suitability of these materials for water treatment applications. The complementary properties of synthetic MOF—characterized by uniform porosity and high stability—and natural coagulants—offering biodegradability and bioactive compounds—suggest potential synergistic effects when used in combination for enhanced turbidity removal and overall water quality improvement. These findings provide a solid foundation for the application of these materials in water treatment systems and highlight the value of integrating synthetic and natural coagulants for optimized performance.

Acknowledgement: The authors wish to appreciate TETFund through the Office of Research and Development, Office of the Vice Chancellor, University of Jos for the IBR Grant number 2017 - 2024/042, which has enabled us to conduct this work.

REFERENCES

1. Adesogan, S. O. & Sasanya, B. F. (2025). Climate-smart water conservation strategy for sustainable development in Nigeria: A systematic review. In R. U. Onyeneke, C. C. Emenekwe & C. U. Nwajiuba (Eds.), Energy transition, climate action and sustainable agriculture. Springer. https://doi.org/10.1007/978-3-031-83165-2_9
2. Ray, K. K., Gunn, L. H., Conde, L. G., Raal, F. J., Wright, R. S., Gosselin, N. H., Leiter, L. A., Koenig, W., Schwartz, G. G., Landmesser, U. & ORION investigators (2024). Estimating potential cardiovascular health benefits of improved population level control of LDL cholesterol through a twice-yearly siRNA-based approach: A simulation study of a health-system level intervention. *Atherosclerosis*, *391*, 117472. https://doi.org/10.1016/j.atherosclerosis.2024.117472
3. Getahun, M., Befekadu, A. & Alemayehu, E. (2024). Coagulation process for the removal of color and turbidity from wet coffee processing industry wastewater using bio-coagulant: Optimization through central composite design. *Heliyon,* 10(7), e27584. https://doi.org/10.1016/j.heliyon.2024.e27584
4. Krupińska, I. (2020). Aluminium drinking water treatment residuals and their toxic impact on human health. *Molecules,* 25(3), 641. https://doi.org/10.3390/molecules25030641
5. Inan-Eroglu, E. & Ayaz, A. (2018). Is aluminum exposure a risk factor for neurological disorders? *Journal of Research in Medical Sciences,* 23, 51. https://doi.org/10.4103/jrms.JRMS_921_17
6. Diver, D., Nhapi, I. & Ruziwa, W. R. (2023). The potential and constraints of replacing conventional chemical coagulants with natural plant extracts in water and wastewater treatment. *Environmental Advances,* 13, 100421. https://doi.org/10.1016/j.envadv.2023.100421
7. Alazaiza, M. Y. D., Alzghoul, T. M., Nassani, D. E. & Bashir, M. J. K. (2025). Natural coagulants for sustainable wastewater treatment: Current global research trends. *Processes,* 13(6). https://doi.org/10.3390/pr13061754
8. Kansal, S. K. & Kumari, A. (2014). Potential of *Moringa oleifera* for the treatment of water and wastewater. *Chemical Reviews*, 114(9), 4993–5010. https://doi.org/10.1021/cr400093w
9. Varsani, V., Vyas, S. J. & Dudhagara, D. R. (2022). Development of bio-based material from *Moringa oleifera*. *Heliyon*, 8(9), e10447. https://doi.org/10.1016/j.heliyon.2022.e10447

10. Ndabigengesere, A. & Subba Narasiah, K. (1998). Quality of water treated by coagulation using *Moringa oleifera* seeds. *Water Research*, 32(3), 781–791. https://doi.org/10.1016/S0043-1354(97)00295-9
11. Delelegn, A., Sahile, S. & Husen, A. (2018). Water purification and antibacterial efficacy of *Moringa oleifera* Lam. *Agric & Food Secur* **7**, 25. https://doi.org/10.1186/s40066-018-0177-1
12. Sarkar, S., Singh, R. P. & Bhattacharya, G. (2021). Exploring the role of *Azadirachta indica* (neem) and its active compounds in the regulation of biological pathways: An update on molecular approach. *3 Biotech*, *11*(4), 178. https://doi.org/10.1007/s13205-021-02745-4
13. Hikaambo, C. , Kaacha, L. , Mudenda, S. , Nyambe, M. , Chabalenge, B. , Phiri, M. , Biete, L. , Akapelwa, T. , Mufwambi, W. , Chulu, M. and Kampamba, M. (2022) Phytochemical Analysis and Antibacterial Activity of *Azadirachta indica* Leaf Extracts against *Escherichia coli*. *Pharmacology & Pharmacy*, 13, 1-10. doi: 10.4236/pp.2022.131001.
14. Khan, Q., Imran, U., Ullman, J. L. & Khokhar, W. A. (2023). Turbidity removal through the application of powdered *Azadirachta indica* (neem) seeds. *Mehran University Research Journal of Engineering & Technology,* 42(1), 1-8. https://doi.org/1022581/muet 1982.2301.01
15. Kaur, H., Devi, N., Siwal, S. S., Alsanie, W. F., Thakur, M. K. & Thakur, V. K. (2023). Metal–organic framework-based materials for wastewater treatment: Superior adsorbent materials for the removal of hazardous pollutants. *ACS Omega,* 8(10), 9004. https://doi.org/10.1021/acsomega.2c07719
16. Thatyana, M., Sihlahla, M. & Mketo, N. (2025). Removal of pharmaceutical pollutants by adsorption onto novel metal–organic frameworks. *Environmental Science and Pollution Research,* 32(50), 28606. https://doi.org/10.1007/s11356-025-37232-3
17. Alamdari, A. (2026). Boosting sono oxidative denitrogenation of fuel over phosphotungstic acid encapsulated into hybrid nano-composites of GO@UiO-66 for indole removal: Process parameters, kinetics, and mechanism. *Carbon Trends,* 23, 100626. https://doi.org/10.1016/j.cartre.2026.100626
18. Sultana N., Priyadarshni P. & Parida K. (2025). UiO-66-NH_2 and Its functional nanohybrides: Unlocking photocatalytic potentials for Clean energy and environmental remediation. *Sustainable Energy fuels.* 2, 3458-3494. Doi: 10.1039/D5SE00150A

19. Xie, H., Xu, M., Liu, M., Zhao, J. & Li, R. (2020). Hydrophobic metal–organic frameworks. *Advanced Science*, 7(4), 1901758. https://doi.org/10.1002/advs.201901758
20. Saito, K., Xu, T. & Ishikita, H. (2022). Correlation between C=O stretching vibrational frequency and pKa shift. *The Journal of Physical Chemistry B*, 126(27), 4999. https://doi.org/10.1021/acs.jpcb.2c02193
21. Zhang, C. Y., Song, H., Huang, F., Ji, T., Zhong, J., Chu, Q. & Xu, W. Q. (2018). UiO-66-NH2/GO composite: Synthesis, characterization and CO2 adsorption performance. *Materials*, 11(4), 589. https://doi.org/10.3390/ma11040589
22. Zavareh, H. S., Pourmadadi, M., Moradi, A., Yazdian, F. & Omidi, M. (2020). Chitosan/carbon quantum dot/aptamer complex as a potential anticancer drug delivery system towards the release of 5-fluorouracil. *International Journal of Biological Macromolecules*, *165*, 1422-1430. https://doi.org/10.1016/j.ijbiomac.2020.09.166
23. Oyeyinka, A. T. & Oyeyinka, S. A. (2018). *Moringa oleifera* as a food fortificant: Recent trends and prospects. *Journal of the Saudi Society of Agricultural Sciences,* 17(2), 127–136.
24. Hong, T., Yin, J. Y., Nie, S. P. & Xie, M. Y. (2021). Applications of infrared spectroscopy in polysaccharide structural analysis: Progress, challenge and perspective. *Food Chemistry*: X, 12, 100168. https://doi.org/10.1016/j.fochx.2021.100168
25. Kwabena Ntibrey, R. A., Kuranchie, F. A. & Gyasi, S. F. (2020). Antimicrobial and coagulation potential of *Moringa oleifera* seed powder coupled with sand filtration for treatment of bath wastewater from public senior high schools in Ghana. *Heliyon*, *6*(8), e04627. https://doi.org/10.1016/j.heliyon.2020.e04627
26. Sabaragamuwa, R. & Perera, C. O. (2023). Total Triterpenes, Polyphenols, Flavonoids, and Antioxidant Activity of Bioactive Phytochemicals of Centella asiatica by Different Extraction Techniques. *Foods*, *12*(21), 3972. https://doi.org/10.3390/foods12213972
27. Ismail, R. M., Salman, H. A. & Ibrahim, H. J. (2024). Study the phytochemical, Biological and pharmacological aspects of *Azadirachta indica* . *GSC Biological and Pharmaceutical Sciences,* 29(1), 033-041. https://doi.org/10.30574/gscbps.2024.29.1.0348
28. Stanciu, I. (2025). Study of the composition of amines using IR spectroscopy. *International Journal of Academic Research and Development*. 10(6), 41-43.

29. Oyekanmi, A. A., Uthaya Kumar, U. S., S, H. P., Olaiya, N. G., Amirul, A. A., Rahman, A. A., Nuryawan, A., Abdullah, C. K. & Rizal, S. (2021). Functional Properties of Antimicrobial Neem Leaves Extract Based Macroalgae Biofilms for Potential Use as Active Dry Packaging Applications. *Polymers*, *13*(10), 1664. https://doi.org/10.3390/polym13101664
30. Verma, A. & Mishra, A. K. (2024). Evaluation of antibacterial properties of neem seed oil. *Journal for Research in Applied Sciences and Biotechnology*, 3(2), 13–16. https://doi.org/10.55544/jrasb.3.2.4
31. Zhang, X., Tian, X., Wu, N., Zhao, S., Qin, Y., Pan, F., Yue, S., Ma, X., Qiao, J., Xu, W., Liu, W., Liu, J., Zhao, M. & Zeng, Z. (2024). Metal-organic frameworks with fine-tuned interlayer spacing for microwave absorption. *Science Advances*, *10*(11), eadl6498. https://doi.org/10.1126/sciadv.adl6498.
32. Liu, S., Dun, C., Yang, F., Tung, K. L., Wierzbicki, D., Ghose, S., Chen, K., Chen, L., Ciora, R., Khan, M. A., Xuan, Z., Yu, M., Urban, J. J. & Swihart, M. T. (2024). A general flame aerosol route to kinetically stabilized metal-organic frameworks. *Nature Communications*, *15*, 9365. https://doi.org/10.1038/s41467-024-53678-4
33. Łuczak, J., Kroczewska, M., Baluk, M., Sowik, J., Mazierski, P. & Zaleska-Medynska, A. (2023). Morphology control through the synthesis of metal-organic frameworks. *Advances in Colloid and Interface Science*, *314*, 102864. https://doi.org/10.1016/j.cis.2023.102864
34. Goji, S. Y. , Jimwan, M. J., Lawal, R. A. & Ago, M. A. . (2024). Integration of Metal Organic Framework (MOFs) into Traditional Coagulation-Flocculation-Sedimentation (CFS) Processes for Enhanced Water Clarification in turbid environment. *Journal of Chemical Society of Nigeria*, *49*(3). https://doi.org/10.46602/jcsn.v49i3.983
35. Thang, V. V., Duy Nguyen, N. T., Nguyen, P. L. & Bac Phung, T. V. (2025). Effective Adsorption of Methyl Orange from Aqueous Solution Using MOFs Nanocomposites UiO-66-NH_2/GO@PVA. *ACS Omega*, *10*(35), 40162. https://doi.org/10.1021/acsomega.5c04958
36. Nurazzi, N. M., M Asyraf, M. R., Rayung, M., F Norrrahim, M. N., Shazleen, S. S., A Rani, M. S., Shafi, A. R., Aisyah, H. A., M Radzi, M. H., Sabaruddin, F. A., Ilyas, R. A., Zainudin, E. S. & Abdan, K. (2021). Thermogravimetric Analysis Properties of Cellulosic Natural Fiber Polymer Composites: A Review on Influence of Chemical Treatments. *Polymers*, *13*(16), 2710. https://doi.org/10.3390/polym13162710
37. Razzak, A., Roy, K. R., Sadia, U. & Zzaman, W. (2022). Effect of thermal processing on physicochemical and antioxidant properties of *Moringa oleifera*. *International Journal of Food Science*, 1502857. https://doi.org/10.1155/2022/1502857.